Research Square

Preprints are preliminary reports that have not undergone peer review.
They should not be considered conclusive, used to inform clinical practice,
or referenced by the media as validated information.

An integrated in silico and in vitro approach for the identification of potent novel PAD4 inhibitors

Priyanka Devi
National Institute of Pharmaceutical Education and Research
Poornachandra Yedla
Jawaharlal Nehru Technological University, Hyderabad
Riyaz Syed
Jawaharlal Nehru Technological University, Hyderabad
Chandraiah Godugu
chandragodugu@gmail.com

National Institute of Pharmaceutical Education and Research

Research Article

Keywords: AI/ML, PAD4 inhibitors, NETosis, inflammation

Posted Date: September 10th, 2026

DOI: https://doi.org/10.21203/rs.3.rs-10867177/v1

License: This work is licensed under a Creative Commons Attribution 4.0 International License.
Read Full License

Additional Declarations: No competing interests reported.

An integrated *in silico* and *in vitro* approach for the identification of potent novel PAD4 inhibitors

Priyanka Devi[1], Poornachandra Yedla[2], Riyaz Syed[2]* and Chandraiah Godugu[1]*

1 Department of Biological Sciences (Pharmacology and Toxicology), National Institute of Pharmaceutical Education and Research (NIPER), Hyderabad

2 Discovery Biology, Centella AI Therapeutics, JTBI, Jawaharlal Nehru Technological University, Hyderabad

***Correspondence:**

Dr. Chandraiah Godugu, Associate Professor,
Department of Biological Sciences (Pharmacology and Toxicology),
National Institute of Pharmaceutical Education and Research (NIPER),
Balanagar, Hyderabad,
Telangana State, India-500037
Telephone: 040-23073741 Fax: 040-23073751
E-mail: chandragodugu@gmail.com, chandra.niperhyd@niperhyd.ac.in

*Co-Corresponding author
Dr. Riyaz Syed,
Discovery Biology,
Centella AI Therapeutics,
JTBI, Jawaharlal Nehru Technological University, Hyderabad
Email: riyaz@centella.ai

Abstract: Peptidyl Arginine Deiminase 4 (PAD4) catalyses the conversion of peptidyl arginine to citrulline resulting in neutrophil extracellular traps (NETs) release, which is known to be elevated in various inflammatory and cancerous conditions. This study aimed to identify potent PAD4 inhibitors by bridging computational design with cell-based biological assays. We screened the Enamine Hit Locator Library of small lead molecules against the PAD4 crystal structure (PDB ID: 8GOD), identifying 25 structurally diverse compounds as final hits. Subsequently, these novel inhibitors significantly inhibited PAD4 enzymatic activity, as evaluated by a PAD4 inhibition assay kit, and controlled NET release in dHL-60 cells. From these assays, we selected two compounds, 16 and 24 for further evaluation in neutrophils and macrophages to assess their activity on NETosis and inflammation. We found that compounds 16 and 24 showed no cytotoxicity in HL60 cells up to 100 μM concentration, indicating their favourable safety profile. Furthermore, our findings demonstrated that these selected compounds suppressed reactive oxygen species (ROS), myeloperoxidase (MPO) and SYTOX Green fluorescence intensities in neutrophils, along with decreased expression of core NETs markers, including PAD4, neutrophil elastase (NE) and citrullinated histone H3 (Cit-H3), which confirm the NETosis-inhibiting effects of novel PAD4 inhibitors. Moreover, NETs isolated from neutrophils after novel inhibitors treatment showed decreased cellular and mitochondrial oxidative stress in RAW264.7 cells. Additionally, macrophages displayed down-regulated expression of TLR4/MyD88 and M1 macrophage polarisation marker along with a reduction in the levels of pro-inflammatory cytokines, which demonstrates that PAD4 inhibition in neutrophils effectively disrupts the inflammatory loop in macrophages that drives tissue damage in various pathological conditions. These results confirm that novel PAD4 inhibitors exhibited both strong anti-NETosis and subsequent anti-inflammatory activity, which represent promising lead compounds for better therapeutic strategies in NET-mediated disease conditions.

Key words: AI/ML, PAD4 inhibitors, NETosis, inflammation.

1. Introduction

Post-translational modification converts peptidyl arginine to peptidyl citrulline in histone by a process known as deimination or citrullination using cysteine hydrolase family of enzymes known as peptidyl arginine deiminases (PADs)[1–4]. Five types of PAD isoforms are known (PAD 1-4 and 6); all of which have enzymatic activity except PAD6. PADs are calcium-dependent enzymes that are involved in the formation of citrullinated proteins that play a role in different physiological processes such as immune response, gene expression and cell signalling, depending on their location. PAD1 participates in epidermal differentiation in skin; PAD2 in glial cells is involved in cytoskeleton degeneration; PAD3 contributes to hair follicle formation; PAD6 has a role in embryonic development in oocytes, embryos and human leukocytes; and PAD4 is a key regulator in the immune response as they are highly expressed in white blood cells (neutrophils, leukocytes, and eosinophils)[3,5,6]. It drives various physiological processes such as cell proliferation and immune response by cytokine production[7–10]. The role of PAD4 was explored in many cancers such as breast cancer, colon cancer, leukaemia and also in various autoimmune disorders[11–14].

Protein citrullination converts the positively charged guanidine group of arginine into neutral citrulline, thereby decreasing the affinity of histone for negatively charged deoxyribonucleic acid (DNA) and facilitating histone dissociation from DNA[15]. PAD4 promotes decondensation of chromatin in neutrophils and thus induces release of intracellular components in the form of neutrophil extracellular traps (NETs) following hypercitrullination of histone H3, H4 and H2A[16]. NETs were first reported by Brinkmann *et al* in 2004 as a reticular structure formed by a network made of a DNA skeleton enveloped with citrullinated proteins and various enzymes such as myeloperoxidases (MPO), neutrophil elastase (NE), cathepsin G and chromosomal DNA coated with other antimicrobial proteins[17,18].

Upon recruitment to an injury site, activated neutrophils eliminate microbes by both phagocytosis and release of their nuclear components, for example, histones, granular enzymes (myeloperoxidase; MPO, neutrophil elastase; NE) and DNA fragments, which result in NET formation to trap and kill pathogens by increasing their interaction with antimicrobial[19,20]. These proteins along with released nuclear and granular components, act as autoantigens and are recognised by antigen-presenting cells (APCs) and initiate the innate immune signalling pathway. In macrophages, these NET components activate Toll-like receptors (TLRs), mainly TLR4, which initiates an intracellular cascade by recruiting myeloid differentiation primary response 88 (MyD88) adapter protein which drives inflammatory pathway by promoting macrophage polarization towards pro-inflammatory M1 phenotype that increases reactive

oxygen species (ROS) production and induces IL-1β, IL-6 and TNF-α production which are major pro-inflammatory cytokines involved in inflammatory conditions[21–24]. This NET-macrophage cross-talk ultimately contributes to tissue damage, indicating the role of this axis in various diseases, including several autoimmune disorders, cystic fibrosis, organ dysfunction in sepsis and multiple coagulopathies where inflammation and tissue damage drive the pathophysiology[18,25–27].

NETs formation as a result of Histone H3 citrullination by PAD4 leads to systemic inflammation and tissue damage[1,28]. Therefore, in order to target NETs, PAD4 inhibition may prove to be a potential target. Several PAD inhibitors have shown good binding for the active site of the enzymes, notably Cl-amidine (CLA), which is a pan-PAD inhibitor that irreversibly causes PAD inhibition through covalent modification in the active site of the protein structure[29,30]. CLA, an irreversible inhibitor of PAD4, normalised symptoms of colitis by reducing inflammation and also improved sepsis survival by suppressing and neutralising citrullinated histones (Cit-H3)[31]. Literature shows that CLA has major effects on neutrophils, which are the primary immune cells[32]. The protective effects of CLA have been proven in several disease pathologies, including collagen-induced arthritis[2,33–35], multiple sclerosis[36], colitis[30], atherosclerosis[31,37,38], lupus[39,40], and kidney injury[41,42]. Recently, a highly specific reversible PAD4 inhibitor, GSK484, which inhibited NET formation in both murine and human cells *in vitro*[43] was found to show protective effects in rheumatoid arthritis[45], colitis[46] and colorectal cancer[43]. Another novel selective PAD4 inhibitor, JBI-589, showed potent efficacy against inflammation in cancer and rheumatoid arthritis[47–49]. Collectively, these studies demonstrate the preclinical efficacy of targeting PAD4 to mitigate inflammation and tissue injury in cancer and immune disorders.

Artificial intelligence (AI) and machine learning (ML) are extensively used tools for accelerated drug discovery as they can process and analyse extensive data sets including protein-protein interactions for target identification, gene expression profiles, molecular docking, and phenotypic screening data[50,51]. AI simulates human intelligence using computer-based models, and ML enables analysis of data to predict outcomes by employing deep learning (DL), which utilises artificial neural networks to learn from intricate data. High-throughput screening (HTS) helps to identify potential drug candidates from the existing large libraries. Ligand interactions with proteins using drug-likeness models help in assessing the bioactivity of molecules for precise compound selection and thereby increasing the chance of successful drug discovery programs [52–54].

In this work, we screened the Enamine Hit Locator Library (HLL) containing diverse small lead molecules based on favourable physicochemical properties against the PAD4 crystal structure (PDB ID: 8GOD) by combining the Auto Dock-GPU scoring function[55] with the ML-based binding prediction model, allowing complementary assessment of docking geometry and interaction quality. Our study integrates molecular docking, virtual, AI-assisted hit prioritisation, and machine learning (ML)-based scoring function (Random Forest method) to screen potential PAD4 inhibitors and also confirm their pharmacological activity in vitro and ex vivo[56]. These approaches helped us to identify 25 molecules as promising leads, which were evaluated for their PAD4 inhibition through a kit-based assay followed by NETs inhibition in differentiated HL-60 (dHL-60) cells, which exhibit a neutrophil-like phenotype. Further, anti-NETosis and anti-inflammatory activity of these novel inhibitors were assessed in neutrophils and macrophages, respectively.

2. Materials and methods

2.1. Protein Structure Preparation and Binding Site Selection

Crystal structures of peptidyl arginine deiminase 4 (PAD4) deposited in the Protein Data Bank (PDB) were examined to identify a suitable binding site for structure-based virtual screening. A total of 21 PAD4 crystal structures, including eleven ligand-bound complexes, were structurally aligned to compare ligand-binding modes and assess conformational variations across available protein structures. Structural comparison showed that most reported inhibitors occupied the canonical substrate binding pocket through arginine mimetic chemotypes[34,57] Whereas alignment of the recently reported PAD4 structure (PDB ID: 8GOD) with the substrate-bound structure (PDB ID: 1WDA) revealed an adjacent pocket directly associated with the substrate-binding region that could potentially accommodate structurally distinct molecules. Analysis of potent PAD4 inhibitors retrieved from ChEMBL[58], which indicated that many high-affinity compounds extended into this neighbouring region. Hence, the adjacent pocket was selected as the target site for virtual screening to enable the identification of chemically diverse PAD4 inhibitors with non-substrate competitive binding modes.

2.2. Dataset Curation and Chemical Space Analysis

Experimentally validated PAD4 inhibitors were curated from the ChEMBL database to characterise the chemical space represented by known ligands. The dataset included 216 molecules that were standardised by harmonising stereochemical representations, neutralising ionisation states, canonicalizing tautomers and removing salts and duplicate entries. For compounds with multiple reported activity measurements, the geometric mean potency was

calculated, whereas entries exhibiting activity differences exceeding one logarithmic unit were excluded from further analysis. Molecular diversity was subsequently assessed by fingerprint-based clustering using a Tanimoto similarity threshold of 0.4[59]. The structural characteristics of highly potent inhibitors (IC_{50} < 100 nM) were then compared with those of moderately active compounds (IC_{50} = 100 nM -10 μM) to identify conserved scaffold features and interaction patterns that directed subsequent compound prioritisation.

2.3. High-Throughput Virtual Screening

The Enamine Hit Locator Library (HLL), consisting of approximately 460,000 lead-like compounds, was selected for virtual screening against the PAD4 protein. Prior to docking, the library was prepared through removal of salts, assignment of appropriate protonation states, generation of 3D conformations, and geometry optimisation. Molecular docking was carried out against the selected PAD4 adjacent binding pocket using AutoDock-GPU[55]. For each molecule, 50 independent docking simulations were performed, and both the lowest predicted binding energy and the lowest cluster energy were retained for compound ranking.

2.4. AI-Assisted Hit Prioritisation and Compound Selection

Docking predictions were further improved by integrating Auto Dock-GPU scores with an in-house supervised machine learning (ML)-based scoring (Random Forest method) model trained on experimentally validated protein-ligand complexes[60]. Each compound was independently evaluated by both approaches, and consensus ranking was used to improve hit prioritisation while reducing false-positive predictions. The top-ranked compounds were subsequently filtered according to docking score, docking cluster consistency, and structural diversity. Structural redundancy was minimised by fingerprint-based clustering using multiple Tanimoto similarity thresholds ranging from 0.3–0.5, after which representative compounds from each cluster were retained. The remaining molecules were manually inspected to verify plausible binding geometries, favourable hydrogen bonding and hydrophobic interactions, and the absence of significant steric clashes within the selected binding pocket.

2.5. Protein-Ligand Interaction Analysis

Binding interactions of the prioritised compounds were analysed to characterise their interactions within the PAD4 binding pocket. Hydrogen bonds, hydrophobic interactions, and residue-level interactions were examined to identify conserved interaction patterns associated with stable ligand binding. The resulting interaction profiles were used to prioritise chemically diverse scaffolds for subsequent experimental validation. Further, the PAD4 amino acid residues that interact with the active compounds were examined.

2.6. Pharmacological Evaluation

2.6.1. Materials

Mouse macrophage cell line RAW264.7 and HL-60 (human promyelocytic leukaemia) cells were procured from the American Type Culture Collection (ATCC, USA). PAD4 inhibitor screening assay kit was supplied by Cayman chemical Chemicals (USA). SYTOX Green, MitoSOX Red staining reagents and enzyme-linked immunosorbent assay kits were purchased from Invitrogen (USA). Cl-amidine (CLA), bovine serum albumin (BSA), JC-1 dye, dichlorofluorescein diacetate (DCFDA), Fluoroshield with DAPI (4′,6-diamidino-2-phenylindole) and Phorbol 12-myristate 13-acetate (PMA) were purchased from Sigma-Aldrich (USA). Histopaque-1077, Histopaque-1119 and Alamar Blue/resazurin were acquired from HiMedia. Bradford reagent and DMF (Dimethylformamide) were procured from SRL Chemicals (India). Antibodies CD86, NE and Cit-H3 were purchased from Cell Signalling Technology (USA), and PAD4 antibody, along with fluorescently-labelled secondary antibodies against mouse and rabbit, were procured from Santa-Cruz Biotechnology (USA). Real-time polymerase chain reaction (RT-PCR) Primers for GAPDH, NE, MPO and PAD-4 were purchased from Eurofins Genomics (France).

2.6.2. Cell culture and treatment

HL-60 cells were maintained in Roswell Park Memorial Institute 1640 (RPMI) medium supplemented with 20% FBS. The murine macrophage cells RAW 264.7 were cultured in Dulbecco's Modified Eagle Medium (DMEM) high glucose medium supplemented with 10% FBS, 100 U/mL penicillin G, and 100 mg/mL streptomycin. The primary neutrophils isolated from mouse blood were maintained in RPMI-1640 medium supplemented with 1% antibiotic solution and 10% FBS. All the cells were maintained in an incubator with 5% CO_2 and a temperature at 37°C. In case of HL-60, cells were differentiated into neutrophil-like dHL-60 cells with 70 mM DMF for 5 days. These differentiated HL-60 cells or primary neutrophils were stimulated with 100 nM PMA (standard inducer of NET) and pre-treatment was given with 10 μM of compounds 16, 24 and 100 μM of CLA (standard inhibitor of PAD4) before 30 min of PMA stimulation. NETs isolation was done from primary neutrophils after PMA stimulation and compound 16, 24 and CLA treatment. RAW264.7 cells were stimulated with NETs isolated from PMA-stimulated or PMA-stimulated and compounds 16, 24 and CLA-treated neutrophils to evaluate the anti-inflammatory effects of compounds 16 and 24 in comparison to standard CLA.

2.6.3. Cell viability/cytotoxicity

Cell viability was evaluated using the resazurin reagent. In a 96-well plate, dHL-60 cells were treated with varying concentrations (10–100 μM) of compounds 16 and 24 for 24h. At the end of the treatment period, resazurin (final concentration 100 mg/L) was added to the plate and incubated for 1h. The fluorescence intensity was measured at an excitation of 530 nm and emission of 590 nm using the Biotek Cytation 5 multi-mode reader.

2.6.4. PAD4 inhibition assay

The PAD4 inhibitory assay was evaluated through the kit-based method. The method was followed as per the instructions given in the manual. Briefly, after the addition of the reagents to the wells, the test inhibitor was added, and the plate was incubated for 5 min at room temperature (RT), followed by reaction initiation through PAD4 substrate and incubation at 37°C for 30 min. 20 μL of PAD stop solution and 10 μL of ammonia detector were added to each well and incubated for 15 min at 37°C. Fluorescence was measured at an excitation wavelength of 405 nm and an emission wavelength of 480 nm. The subsequent PAD4 inhibitory activity was also evaluated through the COLDER (colour development reagent) assay. This assay involves the urea group that is uniquely present in citrulline. This reaction involves the acid-catalysed modification of the urea with diacetylmonooxime in the presence of thiosemicarbazone and ammonium iron(III) sulphate, as well as phosphoric and sulfuric acid. The developed colour was directly proportional to the activity of PAD4.

2.6.5. Experimental animals

6-8 week-old male C57BL/6 mice with 25-30g weight were procured from the National Institute of Preclinical Research (NIPCR) after approval from the Institutional Animal Ethics Committee (IAEC) of NIPER Hyderabad under protocol number (NIP/09/2025/PC/701). Animals were provided free access to feed pellets and water ad libitum and housed in a room with a constant 22 ± 2°C temperature and 12h light/dark cycle.

2.6.6. Isolation of primary neutrophils from mice blood

Neutrophils were isolated using Histopaque double-density gradient centrifugation. Histopaque-1077 was carefully layered on top of Histopaque-1119 in a centrifuge tube, followed by the addition of an equal volume of mouse whole blood. The mixture was then centrifuged at 700 g for 30 min with the brake off to prevent layer disruption. After spinning, the cloudy neutrophil band located at the interface between the two Histopaque layers was harvested. Finally, the collected cells were washed with calcium-free and magnesium-free buffer, and a brief red blood cell lysis step was done to obtain a highly purified neutrophil-rich pellet and re-suspended in fresh complete RPMI media.

2.6.7. SYTOX Green NETosis assay

For the NETosis induction, neutrophils (dHL-60 cells or primary isolated blood neutrophils) were stimulated with 100 nM PMA after pre-treatment for 30 min with 25 novel PAD4 inhibitors (10 μM) along with the standard inhibitor CLA. After 4h, 200 nM SYTOX Green, a cell-impermeable nucleic acid dye, was added to the cells and incubated for 15 min in the dark. The changes in fluorescence intensities were measured at 485 nm excitation and 523 nm emission using the Biotek Cytation 5 multi-mode reader. Images were captured for lead compounds 16 and 24 using a fluorescence microscope (Olympus, BX53F2) at 20X.

2.6.8. Giemsa Staining

To further evaluate the effect of lead compounds 16 and 24 on NET formation, dHL-60 cells were fixed and stained with May-Grunwald solution for 2 min, rinsed with distilled water, and then stained with Giemsa stain (0.4% solution in methanol) for 10 min. The wells were thoroughly rinsed with distilled water and air-dried. Cellular morphology, including chromatin decondensation and membrane integrity, was examined under light microscopy at 40X magnification (Olympus, BX53F2).

2.6.9. cfDNA Concentration

The quantification of cell-free DNA (cfDNA) in neutrophil supernatants, a measure of NET release, was performed using the Quant-iT™ PicoGreen® dsDNA Assay Kit (Invitrogen), which offers high specificity for double-stranded DNA. The protocol involves collecting neutrophil supernatants following centrifugation, followed by a 5 min incubation with PicoGreen working solution, with fluorescence detection at 485 nm excitation and 535 nm emission using a BioTek Cytation 5 multi-mode reader.

2.6.10. Stimulation of the neutrophils and isolation of NETs

NETosis was stimulated in neutrophils using PMA (100 nM) and treated with compounds 16, 24 and CLA for 4h. NETs were isolated from PMA-stimulated neutrophils or PMA-stimulated and treated with compounds 16, 24 and CLA as per our laboratory standardised protocol[61]. Following incubation, the conditioned culture media containing NETs and loose neutrophil layers were carefully collected and centrifuged at 1000 rpm for 10 min, yielding a NET-rich supernatant, which was further centrifuged at 18000 g for 10 min at 4°C, facilitating NET sedimentation and pellet formation. The resulting supernatant was discarded, and the NET pellet was suspended in sterile nuclease-free water to obtain a cell-free NET stock solution, which was used further to evaluate the effect of compounds 16 and 24 on inflammation in RAW264.7 cells.

2.6.11. Measurement of nitrite levels

The anti-inflammatory activity of compounds 16 and 24 was evaluated *in vitro* using RAW264.7 cells by estimating nitrite levels. RAW264.7 cells were incubated with NETs for 24h followed by which the supernatant was collected, and the concentration of nitrite was measured as per laboratory-standardised protocol[59] using Griess reagent. Equal volume of supernatants was incubated with Griess reagent for 10 min, and the absorbance was measured at 540 nm.

2.6.12. Measurement of myeloperoxidase levels

To evaluate MPO levels, cells were harvested and lysed in cold 50 mM potassium phosphate buffer (pH 6.0) containing 0.5% (w/v) hexadecyltrimethylammonium bromide (HTAB). The lysates were centrifuged at 9,168 × *g* for 10 min at 4°C, and the resulting supernatant containing the extracted MPO enzyme was collected. MPO activity was quantified colorimetrically by mixing the supernatant with a reaction buffer containing o-dianisidine dihydrochloride and hydrogen peroxide as the substrate. The rate of o-dianisidine oxidation was determined by measuring the absorbance at 460 nm using a Multiskan SkyHigh microplate spectrophotometer.

2.6.13. Measurement of pro-inflammatory cytokine levels

The levels of pro-inflammatory cytokines, including CCL2, IL-6, IL-1β and TNF-α were quantified in the cell culture media collected from RAW264.7 cells treated with NETs using commercially available mouse ELISA kits (Invitrogen catalogue no. 88–7324, 88–7013, 88–7064, 88-7391, and 88–8350, respectively) according to the manufacturer's protocol.

2.6.14. Morphological evaluation, DCFDA and MitoSOX red staining

RAW264.7 cells were exposed to NETs isolated from compound 16, 24 and standard CLA-treated neutrophils for 24h, and their morphological changes, such as an increase in cell size and development of pseudopodia, were evaluated under bright-field microscopy. Further, cellular and mitochondrial ROS levels were evaluated through DCFDA and MitoSOX red staining techniques, respectively. Following removal of media, cells were incubated with 10 μM of DCFDA or 5 μM of MitoSOX red dye for 30 min at 37^0C in the dark. The fluorescence images were taken using a fluorescent microscope (Nikon Ti2, Japan). The cellular ROS levels were quantified by measuring the fluorescence at an excitation wavelength of 485 nm and emission at 535 nm using the Biotek Cytation 5 multi-mode reader.

2.6.15. Immunofluorescence

Neutrophils and RAW264.7 cells were plated on coverslips in a 6-well plate and cultured in a CO_2 incubator at 37°C. After treatment, cells were fixed with 4% paraformaldehyde for 15 min, washed, permeabilised with 0.1 % Triton X-100 for 15 min and blocked with 3% BSA for 1h.

After another wash, neutrophils were incubated with primary antibodies against PAD4, Cit-H3 and NE antibodies and RAW 264.7 cells with TLR4, MyD88 and CD86 antibodies. The next day, cells were washed and incubated with FITC-conjugated anti-mouse and rhodamine-conjugated anti-rabbit secondary antibodies for 1h in the dark. Cells were mounted using Fluoroshield mounting media with DAPI and observed under fluorescence microscopy. The images were taken at 40X magnification (Olympus, BX53F2).

2.6.16. RT-PCR analysis

After stimulation of neutrophil-like dHL-60 cells with PMA (100 nM) and treatment with compound 16, 24 and standard CLA for 4h. RNA isolation kit was used to isolate total RNA from the cell lysates using RNAiso Plus (Takara, Japan). Complementary DNA (cDNA) was synthesised from the RNA using the PrimeScript 1st strand cDNA synthesis kit (Takara, Japan). Quantitative real-time PCR (qPCR) amplification of cDNA was performed in a CFX96 Real-Time PCR detection system (Bio-Rad, USA) using the TB Green Premix Ex Taq II qPCR kit (Takara, Japan). Primer sequences are listed below. GAPDH was used as an internal standard, and fold change was calculated.

Table 1: *List of primer sequences used for RT-PCR analysis.*

Gene	Forward primer (5'- 3')	Reverse primer (5'- 3')
GAPDH	GGTGAAGGTCGGTGTGAACG	CCCGTAGGGCGATTACAGTC
PAD-4	TCTGCTCCTAAGGGCTACACA	GTCCAGAGGCCATTTGGAGG
NE	ACTGTGTGAACGGCCTAAAT	CTGGGTGATGGTCTGTTTGT
MPO	TCCCGGTATGTGATGATCTG	TCGATGGAATGGGGAGAA

2.6.17. Statistical analysis

All the results are represented as mean ± SEM of three independent experiments. Statistical analysis was performed by ANOVA and Tukey's post hoc test. All statistical analyses were carried out using GraphPad Prism® Version 8 software. A *p-value* of less than 0.05 ($p<0.05$) was considered statistically significant.

3. Results

3.1. Molecular docking analysis

3.1.1. Binding Pocket selection for PAD4 Inhibitor Design

Structural comparison of the 21 available PAD4 crystal structures showed that most reported inhibitors bind within the canonical substrate binding pocket through arginine-mimetic scaffolds[57]. Among the 11 ligand-bound structures, only three contained non-arginine

chemotypes, indicating that previous inhibitor development has largely focused on the substrate-binding region while adjacent binding sites remain relatively less explored. Alignment of the recently reported PAD4 structure (PDB ID: 8GOD) with the substrate-bound complex (PDB ID: 1WDA) identified a neighbouring pocket connecting with the catalytic site that can accommodate structurally distinct ligands. Analysis of 216 experimentally validated PAD4 inhibitors collected from ChEMBL further revealed that highly active compounds preferentially extended into this adjacent region, whereas inhibitors with moderate activity displayed less consistent occupancy. Collectively, our findings supported the selection of the adjacent pocket as the target site for subsequent virtual screening and AI-assisted hit discovery.

3.1.2. Chemical Space Analysis of Known PAD4 Inhibitors

The curated dataset of 216 PAD4 inhibitors was analysed to evaluate the structural diversity of reported chemotypes. Fingerprint-based clustering using a Tanimoto similarity threshold of 0.4 partitioned the dataset into 39 representative scaffold clusters, indicating that known PAD4 inhibitors are focused within a relatively restricted region of chemical space despite apparent structural diversity. Comparison of highly potent inhibitors (IC_{50} < 100 nM) with compounds exhibiting moderate activity (100 nM - 10 μM) identified conserved structural features associated with increased potency.

3.1.3. AI-Assisted Virtual Screening and Consensus-Based Hit Prioritisation

The Enamine HLL library was screened against the selected adjacent PAD4 binding pocket. Compounds were initially evaluated based on their lowest binding energy and lowest cluster energy, followed by rescoring with an in-house supervised machine learning model trained on experimentally validated protein–ligand complexes. Consensus ranking integrating both docking and machine learning scores was used to prioritise compounds with favourable predicted binding affinity, reproducible binding poses, and protein–ligand interaction profiles. Based on the combined virtual screening and consensus scoring workflow, the top 10,000 compounds were selected for further analysis. The prioritised set exhibited a broad distribution of predicted binding affinities together with consistent docking pose convergence, supporting the reliability of the AI-assisted hit identification strategy.

3.1.4. Scaffold Diversity and Selection of Final Hit Compounds

The highest-ranked 10,000 compounds were further subjected to fingerprint-based clustering using extended connectivity fingerprints (ECFP) and Tanimoto similarity to remove structurally redundant molecules while preserving scaffold diversity. At a Tanimoto similarity threshold of 0.3, application of a docking pose consistency criterion requiring 45 of 50 poses to converge produced 918 representative scaffold clusters. Increasing the similarity threshold

to 0.4 and 0.5 reduced the number of representative clusters to 865 and 754, respectively. Applying a more stringent criterion requiring complete convergence of all 50 docking poses yielded 116, 113, and 111 representative compounds at Tanimoto thresholds of 0.3, 0.4, and 0.5, respectively. These candidates were subsequently evaluated by medicinal chemistry review and detailed visual inspection of their predicted binding modes. Based on docking geometry, pose consistency, and favourable interactions within the adjacent PAD4 pocket, 25 structurally diverse compounds were selected as the final hit set for experimental validation.

3.1.5. Protein-Ligand Interaction Analysis

The most active compounds (16 and 24) from the experimental results were examined for docking analysis with the PAD4 protein (8GOD) co-crystallised with K3X to identify the key PAD4 residues involved in ligand binding. The docked ligands bound to the PAD4 by both hydrogen and hydrophobic interactions and displayed good binding energy. For each docked ligand, ten different binding poses were generated, and the top-ranked conformation was shown in **Figure 1**. Docking analysis predicted that compounds 16 and 24 bind to PAD4 with a binding energy of - 9.8 kcal/mol and -9.76 kcal/mol, respectively, which were comparable to that of the co-crystallised ligand K3X (−9.7 kcal/mol). Compound 16 formed two hydrogen bonds with Phe633 and Phe634, while compound 24 formed hydrogen bonds with Asn585 and Asn588 in the PAD4 binding pocket. Both hydrogen and hydrophobic interactions influenced the binding energy results. The amino acid residues of the PAD4 that interacted with the docked ligands were shown in **Table 2**.

Table 2: *Amino acid residues of the PAD4 protein interacting with the docked ligands through hydrogen bonding and hydrophobic interactions, along with their predicted binding energies.*

Ligand	**Binding Energy (Kcal/mol)**	**Protein–Ligand interactions**	
		H-bond/s	**Hydrophobic bonds**
16	-9.85	Phe633, Phe634	Val643, Phe602, Ile518, Asp632, Pro584, Asn585
24	-9.76	Asn588, Asn585	His644, Asp350, Glu474, Phe634, Ala581, Pro584, Val469, Val643, Cys645
K3X (Co-crystal ligand)	-9.79	Val643	Asn585, Asn588, Phe634, Pro584, Phe 633, Lys600, Phe602, Asp632, Thr635, Glu474, Ala581

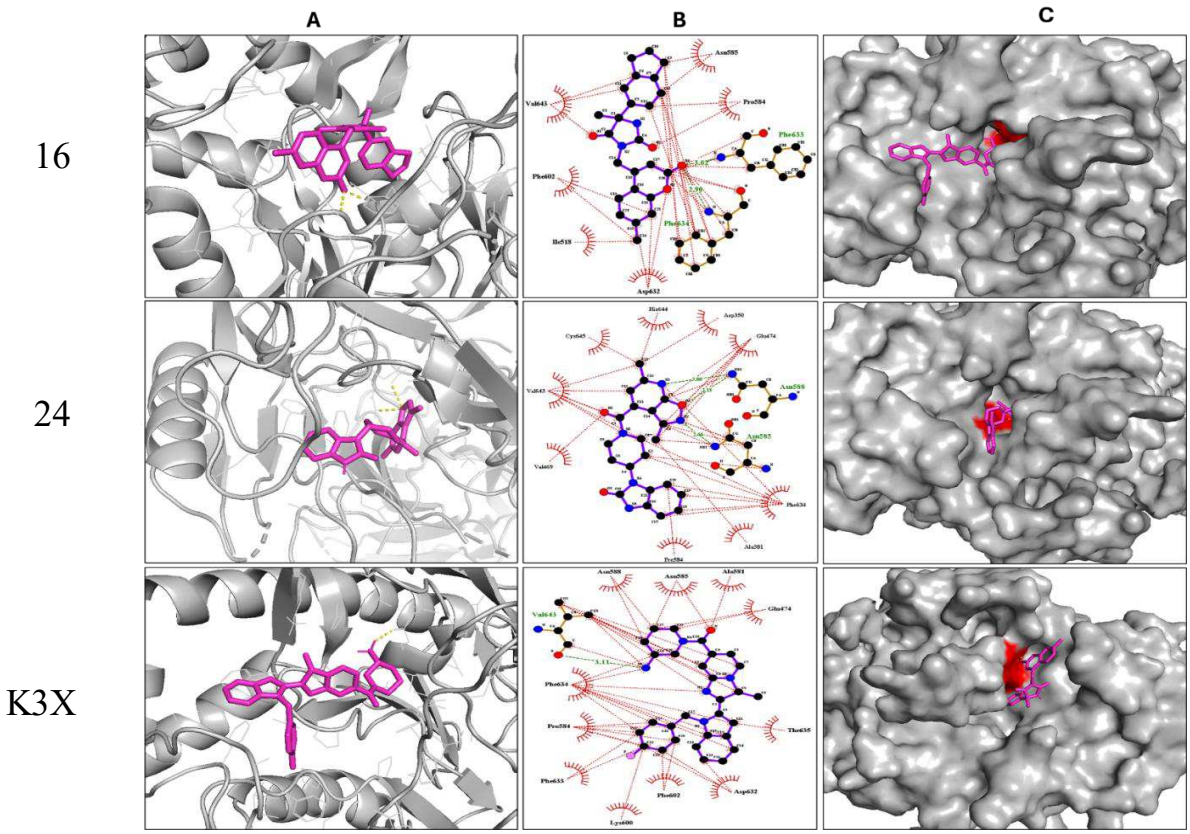


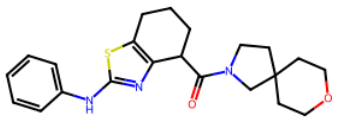
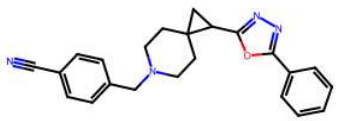
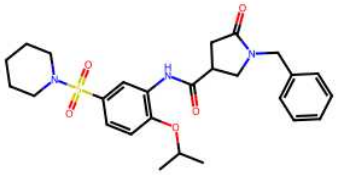
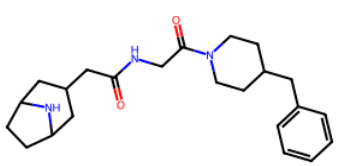
Figure 1: ***(A)*** *3D binding conformations of the compounds 16 and 24 against the PAD4 protein (PDB ID: 8GOD). The yellow dashed lines are indicating the hydrogen bond interactions,* ***(B)*** *Both hydrogen and hydrophobic interactions of the docked ligand with the target protein and* ***(C)*** *Surface representation of the docked compound along with the co-crystallised ligand in the protein active site.*

3.2. Pharmacological Evaluation

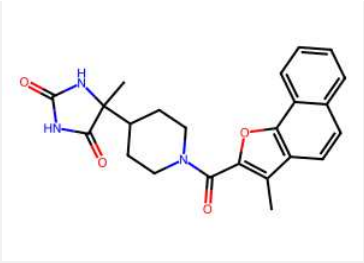
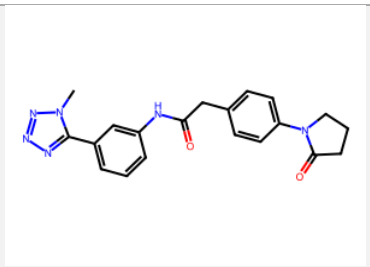
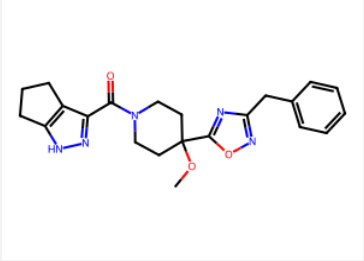
3.2.1. PAD4 and NETs inhibition of the novel PAD4 inhibitors in neutrophil like dHL-60 cells

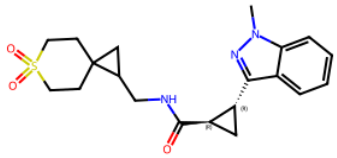
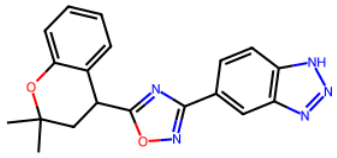
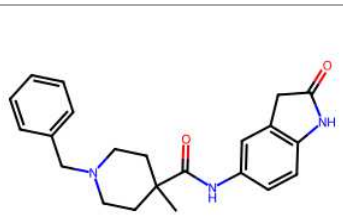
25 hit molecules were screened for PAD4 and NETs inhibitory potential using a cell-free PAD4 enzymatic assay kit and PMA-stimulated neutrophil-like dHL-60 cells. We evaluated the PAD-4 enzyme inhibitory activities through a kit-based enzyme inhibition assay, where we found that the IC_{50} values of lead molecules 16 and 24 were 0.18±0.01 µM and 3.07±0.17 µM, respectively, in comparison to the standard CLA with an IC_{50} value of 6.45±0.27 µM. Furthermore, we differentiated the HL-60 cells with 70mM DMF and evaluated the percentage of SYTOX Green inhibition by novel PAD4 inhibitors to determine the reduction of PMA-stimulated NETs formation, where lead molecules 16 and 24 (10 µM) showed 48.18±3.8 and 27.26±5.04% NET-inhibition, respectively, in comparison to 10.87±1.65% in the case of standard CLA (100 µM). The newly discovered PAD4 inhibitors (16 and 24) exhibit exceptional potency compared to standard CLA in both the cell-free enzymatic level and cellular anti-NETosis efficacy at a ten-fold lower concentration **(Table 3)**.

Table 3: *PAD4 enzyme inhibition and percentage of NETs inhibition by the novel inhibitors. All the results are presented as mean ± SEM. Compound 16 (highlighted green) is the most potent PAD4 inhibitor (IC_{50} 0.81±1.48 µM) with highest % SYTOX Green inhibition (48.18±3.80%) in dHL-60 cells. Reference compound: Cl-amidine (CLA). Source: PAD4.xlsx + pad4_structures_with_smiles.pdf*

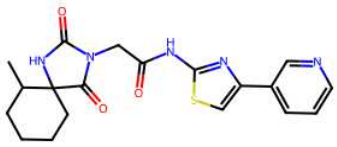
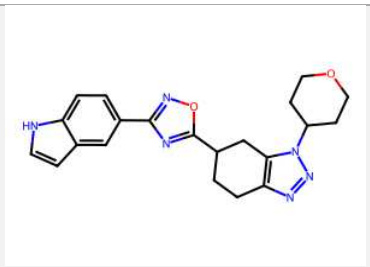
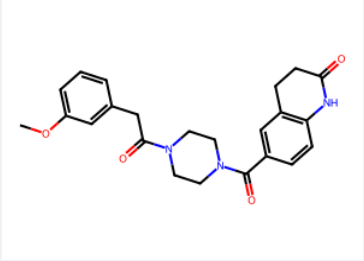
PAD4 Inhibitor Structures & Biological Activity — Mapped Data				
S. No	**Structure**	**SMILES**	**PAD4 IC_{50} (µM)**	**SYTOX Green Inhibition (%) at 10 µM**
1		O=C(C1CCCC=2SC(=NC21)NC=3C=CC=CC3)N4CCC5(C4)CCOCC5	7.59±0.80	10.81±0.80
2		O=C(CCCC=1C=CC=CC1)N2CCN(CC2)C(=O)CC3CC4CCC(C3)N4	20.46±1.45	11.38±3.60
3		N#CC=1C=CC(=CC1)CN2CCC3(CC3C4=NN=C(O4)C=5C=CC=CC5)CC2	8.46±0.35	11.46±2.73
4		CC(C)OC=1C=CC(=CC1NC(=O)C2CC(=O)N(CC=3C=CC=CC3)C2)S(=O)(=O)N4CCCCC4	6.15±0.21	12.19±7.55
5		O=C(CC1CC2CCC(C1)N2)NCC(=O)N3CCC(CC=4C=CC=CC4)CC3	3.22±0.01	12.20±3.56

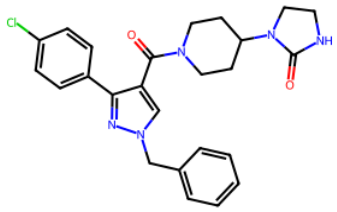
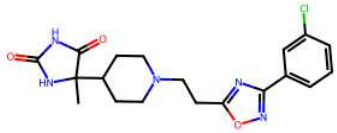
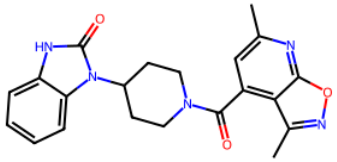
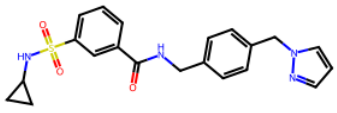
PAD4 Inhibitor Structures & Biological Activity — Mapped Data

S. No	Structure	SMILES	PAD4 IC_{50} (µM)	SYTOX Green Inhibition (%) at 10 µM
6		CC1=C(OC=2C1=CC=C3C=CC=CC23)C(=O)N4CCC(CC4)C5(C)NC(=O)NC5=O	4.13±0.33	12.82±5.27
7		CC=1C=CC(=CC1)C2CC(C)N(C2)C(=O)NC=3C=CC=C(C3)N4CCCNC4=O	9.97±1.31	12.93±5.23
8		CN1N=NN=C1C=2C=CC=C(C2)NC(=O)CC=3C=CC(=CC3)N4CCCC4=O	7.70±0.03	13.19±2.50
9		O=C(NC=1C=CC=C(C1)N2CCNC2=O)C=3C=CC=C(C3)CN4CCCC4	9.62±2.28	14.45±3.20
10		COC1(CCN(CC1)C(=O)C2=NNC=3CCCC23)C4=NC(CC=5C=CC=CC5)=NO4	5.62±0.24	14.65±3.70

PAD4 Inhibitor Structures & Biological Activity — Mapped Data				
S. No	**Structure**	**SMILES**	**PAD4 IC_{50} (µM)**	**SYTOX Green Inhibition (%) at 10 µM**
11		O=C(NCC1CCCC1NC(=O)C=2C=CC=3NN=CC3C2)C=4C=CC=5NN=CC5C4	3.99±0.28	14.96±1.08
12		CN1N=C(C=2C=CC=CC21)[C@@H]3C[C@H]3C(=O)NCC4CC54CCS(=O)(=O)CC5	8.81±0.42	15.29±3.89
13		CC1(C)CC(C2=NC(=NO2)C=3C=CC=4NN=NC4C3)C=5C=CC=CC5O1	4.84±0.56	15.95±4.47
14		CC1(CCN(CC=2C=CC=CC2)CC1)C(=O)NC=3C=CC=4NC(=O)CC4C3	8.38±0.13	16.34±3.60
15		NC(=O)C=1C=CC(=CC1)NC(=O)C=2C=CC=C(C2)S(=O)(=O)N(CC=3C=CC=CC3)C=4C=CC=CC4	9.83±3.60	17.04±2.55

PAD4 Inhibitor Structures & Biological Activity — Mapped Data

S. No	Structure	SMILES	PAD4 IC_{50} (µM)	SYTOX Green Inhibition (%) at 10 µM
16		CC=1C=CC=2C(=CC(=O)OC2C1)CN3C(=O)NC(C)(C3=O)C=4C=CC=5CCCC5C4	**0.81±1.48**	**48.18±3.80**
17		CC1CCCCC21NC(=O)N(CC(=O)NC3=NC(=CS3)C=4C=CC=NC4)C2=O	7.39±0.88	18.30±5.58
18		C1=CC=2C=C(C=CC2N1)C3=NOC(=N3)C4CCC=5N=NN(C5C4)C6CCOCC6	11.37±0.23	18.33±5.88
19		CC=1C=CC(=CC1F)C2=NOC(=N2)C(C)N3CCC(C3)NC=4C=CC=CC4	7.36±0.30	18.90±3.09
20		COC=1C=CC=C(C1)CC(=O)N2CCN(CC2)C(=O)C=3C=CC=4NC(=O)CCC4C3	5.75±0.19	19.37±3.97

PAD4 Inhibitor Structures & Biological Activity — Mapped Data				
S. No	**Structure**	**SMILES**	**PAD4 IC_{50} (µM)**	**SYTOX Green Inhibition (%) at 10 µM**
21		O=C(C1=CN(CC=2C=CC=CC2)N=C1C=3C=CC(Cl)=CC3)N4CCC(CC4)N5CCNC5=O	8.74±0.07	19.90±6.75
22		CC1(NC(=O)NC1=O)C2CCN(CCC3=NC(=NO3)C4=CC=CC(Cl)=C4)CC2	10.78±0.02	34.54±7.44
23		CN(C)S(=O)(=O)C=1C=CC2=C(C1)OC(=O)N2CC3=NC(CC=4C=CC=CC4)=NO3	9.64±1.33	6.92±3.76
24		CC1=NOC=2N=C(C)C=C(C(=O)N3CCC(CC3)N4C(=O)NC5=CC=CC=C54)C12	3.07±0.17	27.26±5.04
25		O=C(NCC=1C=CC(=CC1)CN2C=CC=N2)C=3C=CC=C(C3)S(=O)(=O)NC4CC4	7.76±0.02	24.37±5.16
Ref	***Cl-amidine (CLA)***		**6.45±0.27**	**10.87±1.65**

3.2.2. Novel PAD4 inhibitors did not induce cytotoxicity in HL-60 cells

We performed cytotoxicity assays of the selected lead molecules 16, 24 and CLA in HL-60 cells, where we observed that there was no cell toxicity in the concentration range of 0-100 µM after 24h incubation, indicating an excellent safety profile of lead molecules in HL-60 cells with an IC_{50} value above 100 µM, in comparison to standard CLA with IC_{50} value of 5.11±0.24 µM **(Figure 2)**.

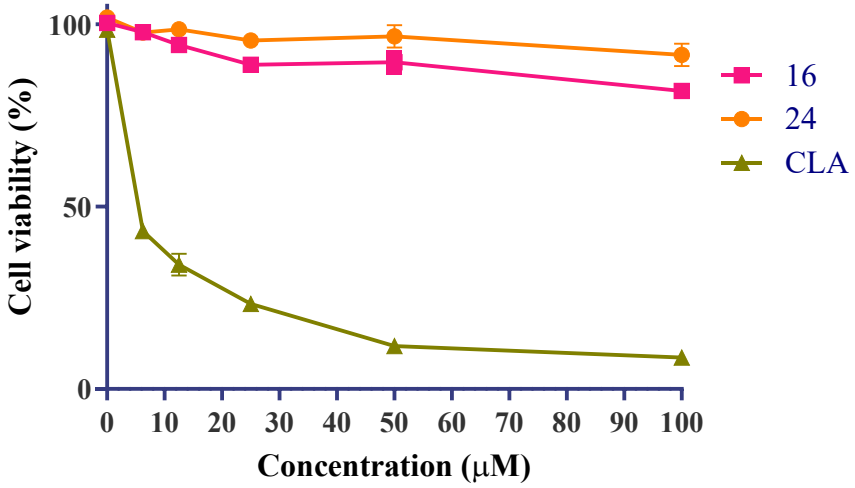


Figure 2*: Line graphs showing the effect of two selected compounds 16, 24 and CLA on the cell viability of HL-60 cells after 24h treatment. Both novel inhibitors demonstrated no cell death, showing favorable safety compared to standard CLA.*

3.2.3. Novel PAD-4 inhibitors decreased NETs release in dHL-60 cells

The NETs release was detected by bright-field (Giemsa) and fluorescence (SYTOX Green and DCFDA) stainings. HL-60 cells were differentiated into neutrophil-like cells using DMF, followed by stimulation with PMA (100 nM) for 4h to induce NETosis, where pre-treatment with novel PAD4 inhibitors along with standard CLA showed reduced intensity of DCFDA in both fluorescence imaging and quantification by fluorescence intensity. These findings indicate that compounds 16 and 24 exhibited PAD4 dependent inhibition of intracellular ROS in dHL-60 cells **(Figure 3A-B)**.

SYTOX Green imaging showed abundant extracellular DNA web structures after PMA stimulation, as evidenced by increased fluorescence intensity. However, treatment with compounds 16 and 24 significantly reduced fluorescence intensity, with both NCEs showing significant NET-inhibiting effects **(Figure 3A lower panel)**. Giemsa staining showed increased formation of extruded web-like meshwork in PMA, whereas compounds 16 and 24-treated neutrophils showed significant reductions in NETs meshwork **(Figure 3A middle panel)**. Additionally, as cfDNA is a by-product of NETosis, cfDNA quantification was performed,

which showed that cfDNA associated with NETs increased significantly after PMA induction and was significantly reduced in compounds 16 and 24-treated cells, suggesting that novel PAD4 inhibitors have suppressed NETosis process **(Figure 3C)**.

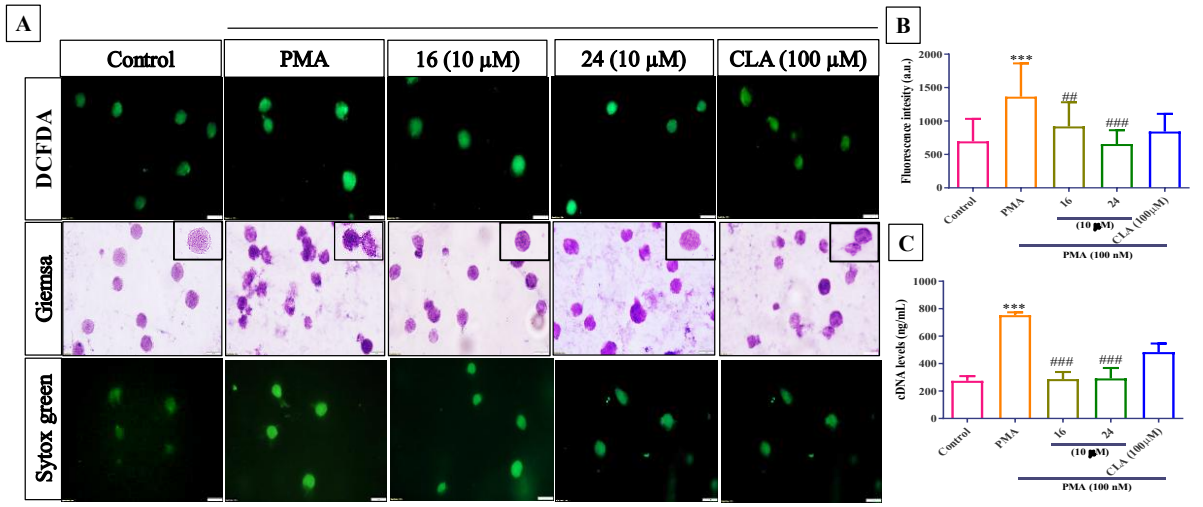


Figure 3: *Effect of selected compounds 16, 24 and CLA on* ***(A)*** *ROS production indicated by DCFDA fluorescence (upper), Giemsa (middle) and SYTOX Green (lower) stainings in dHL60 cells. The images were taken at 40X magnification,* ***(B)*** *Fluorescence intensity of DCFDA and* ***(C)*** *cfDNA levels. All the results are presented as mean ± SEM (n=3). ***p<0.001 vs control and ###p<0.001; ##p<0.01 vs PMA.*

3.2.4. Novel PAD4 inhibitors decreased NETosis markers in dHL-60 cells

Further, we evaluated the NETosis inhibition by compounds 16 and 24 in dHL-60 cells through immunocytochemistry analysis of NET markers, including PAD4, Cit-H3 and NE expression. PMA-induced release of citrullinated products of histones during formation of NETs, which was inhibited by compounds 16 and 24 as evidenced by increase in NETs release and immunopositivity of NETs markers to higher intensity in PMA-stimulated cells, which was significantly reduced by compounds 16 and 24 treatment **(Figure 4)**. Immunofluorescence-based co-localisation of PAD4, Cit-H3 **(Figure 4A)** and NE **(Figure 4B)** with extracellular DNA verified the presence of NET structures in PMA, whereas fluorescence intensity was reduced with compounds 16 and 24. Additionally, we found that mRNA fold changes of NE, MPO and PAD4 increased several fold in the case of PMA-stimulated cells, which were significantly reduced in cells treated with compound 16 **(Figure 4C-E)**. MPO levels in neutrophils were also significantly reduced after treatment with compounds 16 and 24 compared to the PMA-alone group **(Figure 4F)**. Overall, the significant reduction of extracellular NET markers such as MPO, Cit-H3, and NE following PAD4 inhibition underscores the pivotal role of histone hypercitrullination in the release of granular proteins during the execution of NETosis.

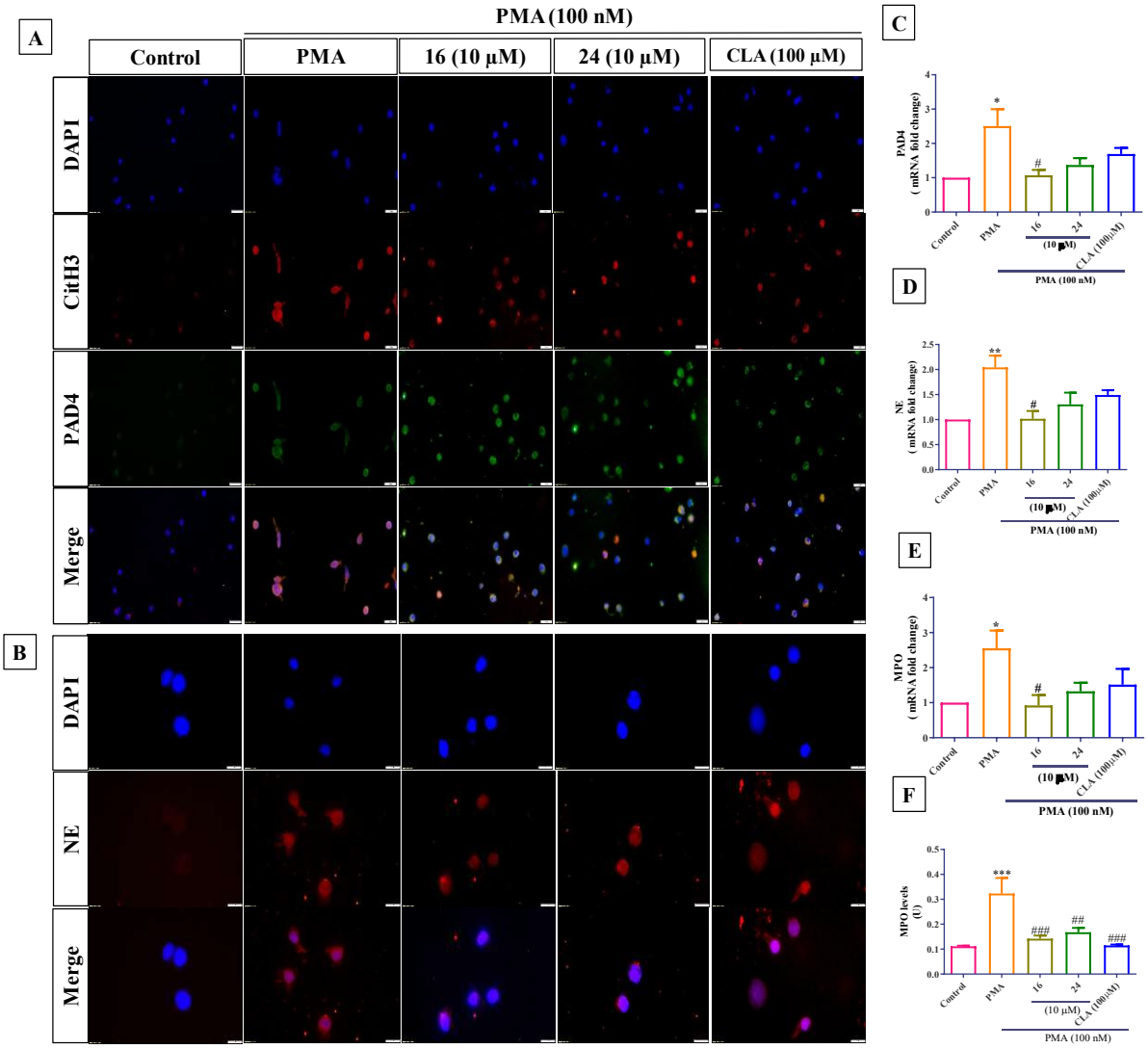


Figure 4: *Effects of selected compounds 16, 24 and CLA on the expression of* ***(A)*** *Cit-H3 and PAD4,* ***(B)*** *neutrophil elastase (NE) markers in dHL-60 cells. The images were taken at 40X magnification,* ***(C-E)*** *mRNA expression of MPO, NE and PAD4 and* ***(F)*** *MPO levels. All the results are presented as mean ± SEM of n=3. ***p<0.001, **p<0.01; *p<0.05 vs control and ###p<0.001; ##p<0.01; #p<0.05 vs PMA.*

3.2.5. Novel PAD4 inhibitors attenuated NETs release in primary neutrophils

We then isolated primary neutrophils from blood collected from mice using a histopaque density gradient and exposed them to compounds 16 and 24. We first estimated the effects of NCEs pre-treatment on the SYTOX Green fluorescence intensity in the primary neutrophils. Neutrophils challenged with PMA exhibited a robust, time-dependent escalation in fluorescent signal intensity, indicating a massive extrusion of expansive extracellular DNA frameworks. Conversely, pre-treatment with the compounds 16 and 24 significantly attenuated this increased fluorescence **(Figure 5A-B)**. In addition, cells exposed to PMA showed higher intensity of NETs markers, both PAD4 expression and the structural NET marker, NE, indicating higher NETosis. However, a reduction in fluorescence intensity was observed upon treatment with the

compounds 16 and 24 (10 µM) and CLA (100 µM) **(Figure 5C)**. MPO levels were also suppressed in compounds 16 and 24-treated neutrophils in comparison to PMA-stimulated cells **(Figure 5D)**. Overall, our results indicate that novel PAD4 inhibitors reduced NET-related markers significantly. The simultaneous suppression of an epigenetic editing enzyme (PAD4) and a primary granular protease (NE) provides strong evidence that targeting PAD4 arrests the overall NETosis process.

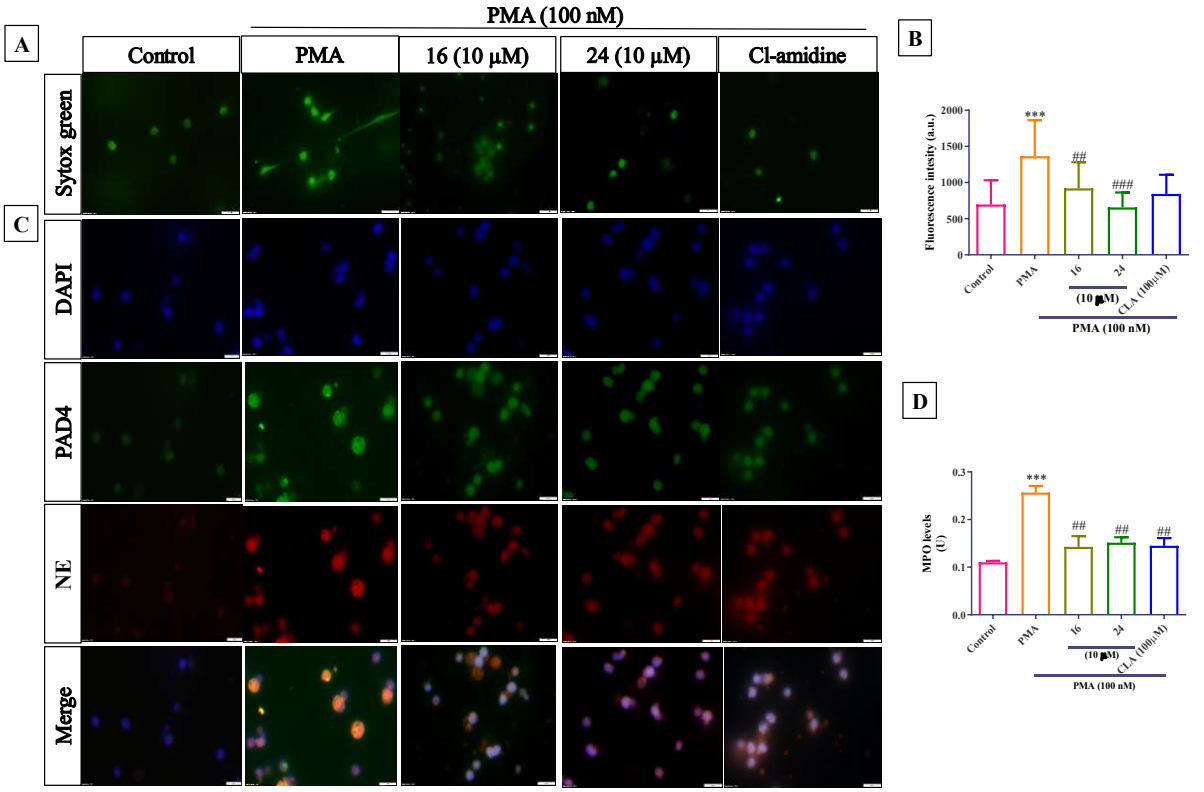


Figure 5: *Effect of the selected compounds 16, 24 and CLA on NETosis markers in primary neutrophils* ***(A)*** *SYTOX Green staining,* ***(B)*** *Graphical representation of fluorescence intensity of SYTOX Green,* ***(C)*** *Representative immunofluorescence images of PAD4 and NE expression. The images were taken at 20X and 40X magnification and* ***(D)*** *MPO levels. All the results are presented as mean ± SEM (n=3). ***p<0.001 vs control and ##p<0.01; ###p<0.001 vs PMA.*

3.2.6. Novel PAD4 inhibitors-induced NET inhibition improved morphology and reduced oxidative stress in macrophages

Based on the macrophage capability to internalise NETs and produce oxidative stress, we then evaluated the effect of NETs isolated from compound 16, 24 and standard CLA-treated neutrophils on macrophage's oxidative levels. NETs isolated from PMA-stimulated neutrophils resulted in altered morphology of RAW264.7 macrophages where extended, irregular cytoplasmic pseudopodia were observed indicating their activated, stressed and phagocytic state trying to engulf sticky extracellular DNA structures. Moreover, they showed increased cellular and mitochondrial oxidative stress. NETs isolated from compound 16, 24 and standard

CLA-treated neutrophils maintained their resting predominantly rounded or slightly amoeboid with well-defined boundaries with no development of pseudopodia **(Figure 6A upper panel)**. Microscopy of DCFDA-stained macrophages revealed increased intracellular oxidative stress after exposure to NETs isolated from compound 16, 24 and standard CLA-treated neutrophils, in comparison to cells subjected to NETs isolated after PMA stimulation **(Figure 6A lower panel)** and also reflected reduced mitochondrial ROS levels when stained with MitoSOX red dye (mitochondrial superoxide indicator), which is consistent with reduced NETs burden in neutrophils **(Figure 6A middle panel)**. Additionally, this data was supported by a significant increase in nitrite and MPO levels in PMA-stimulated NETs, which was suppressed in NETs isolated from compound 16, 24 and standard CLA-treated neutrophils **(Figure 6B-C)**. Overall, the dramatic elevation of cytosolic ROS and mitochondrial superoxides observed in NETs-exposed RAW264.7 cells was effectively abolished under PAD4 inhibition, confirming that PAD4-inhibited neutrophils-treated macrophages remain morphologically intact and maintain cellular, mitochondrial oxidative stress and homeostasis.

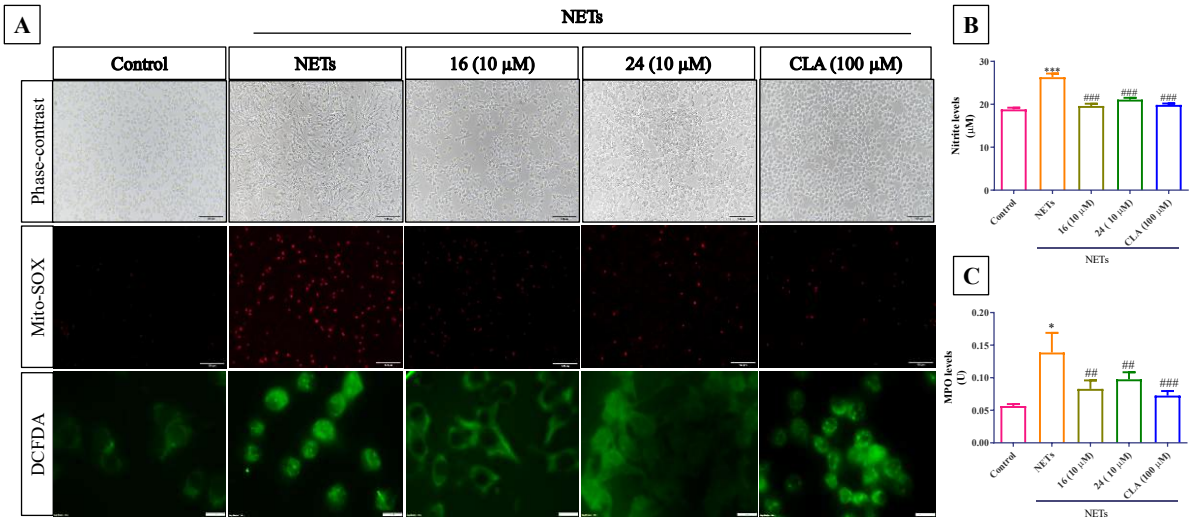


Figure 6: *Effect of NETs isolated from compound 16, 24 and standard CLA-treated PMA-stimulated neutrophils on* ***(A)*** *Morphology, mitochondrial and cellular ROS levels in RAW264.7 macrophages. Images were taken at 20X magnification,* ***(B)*** *Nitrite and* ***(C)*** *MPO levels. All the results are expressed as mean ± SEM (n=3). ***p<0.001; *p<0.05 vs control and ###p<0.001; ##p<0.01 vs NETs.*

3.2.7. Novel PAD4 inhibitors attenuated NET-mediated macrophages polarisation

To evaluate whether NETs isolated from compound 16, 24, and standard CLA-treated neutrophils directly cause inflammation in macrophages, we treated RAW264.7 cells with isolated NETs from PMA–stimulated neutrophils[61]. As per earlier reports, macrophage polarisation gets initiated by activation of TLR4/MyD88 signalling following recognition of NET proteins as autoantigens by TLR4 receptors, initiating inflammatory cross-talk between

neutrophils and macrophages[62]. RAW264.7 macrophages after exposure to PMA-induced NETs showed enhanced TLR4/MyD88 expression along with upregulation of M1 macrophage marker CD86. On the other hand, macrophages challenged with NETs isolated from compound 16, 24 and CLA-treated neutrophils resulted in a significant downregulation of inflammatory proteins TLR4, MyD88 and CD86 expression **(Figure 7A-B)**. Moreover, we found that PMA-stimulated NETs induced the release of pro-inflammatory cytokine levels like CCL2, TNF-α, IL-1β, and IL-6, which were significantly diminished in macrophages exposed to compound 16 and 24-treated NETs compared to CLA **(Figure 7C-F)**, highlighting the effect of NETs on inflammation in macrophages is dependent on PAD4-mediated chromatin decondensation.

Our findings demonstrate that treating neutrophils with novel PAD inhibitors alters their downstream interaction with macrophages. In the absence of compound 16 and 24, PMA-induced NETs acted as an immune stimulator that drove macrophages toward a pro-inflammatory (M1 or activated) phenotype by activating TLR4/MyD88 signalling. Overall, by inhibiting PAD-mediated histone hypercitrullination in the neutrophils, we effectively observed a significant reduction in inflammatory signalling in the macrophages.

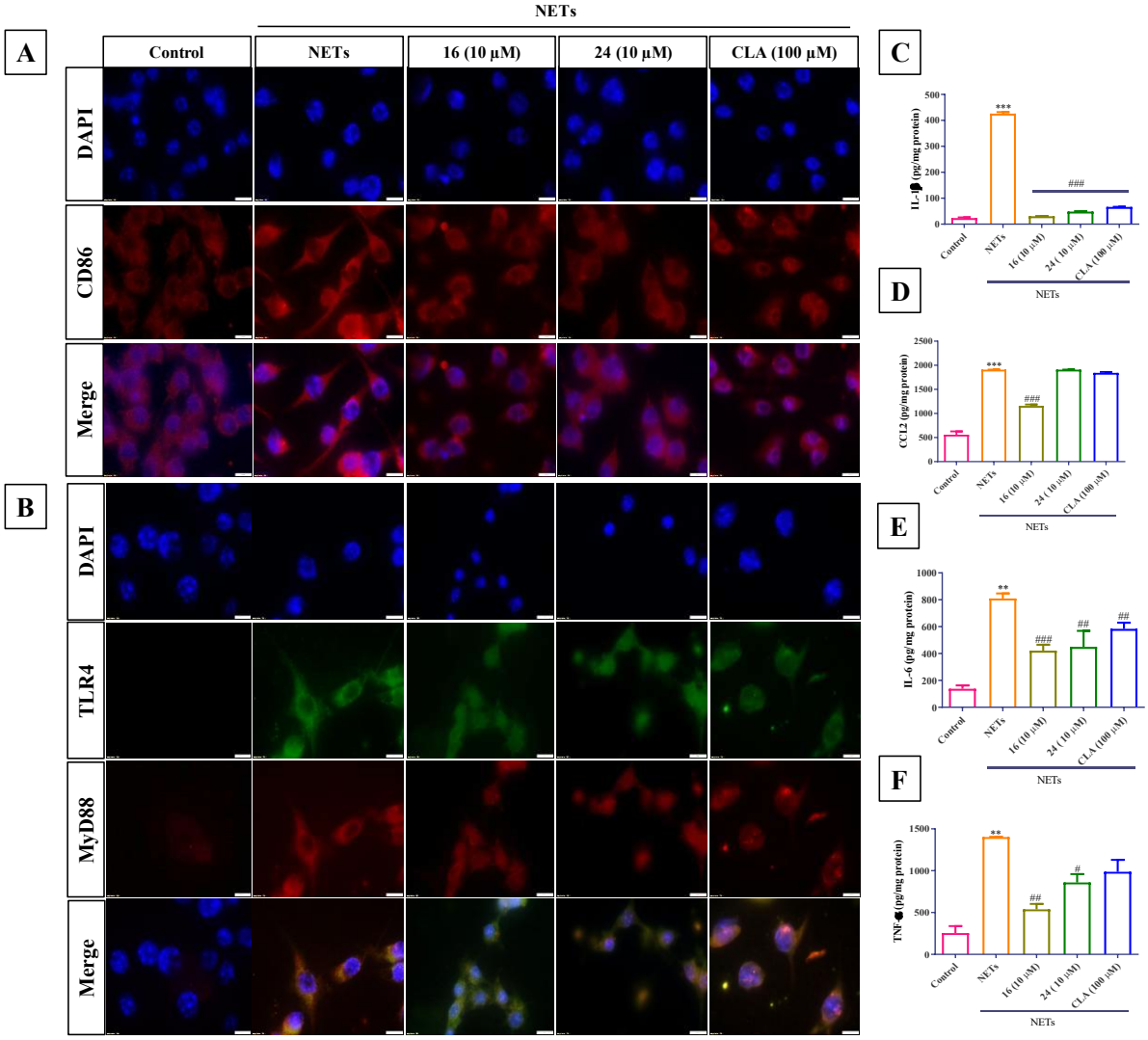


Figure 7: *Representative images of immunofluorescence staining of* ***(A)*** *CD86,* ***(B)*** *TLR4/MyD88 in RAW macrophages after treatment with NETs isolated from PMA-stimulated and compound 16, 24 -treated neutrophils by fluorescence microscopy. Scale bar: 50 µm and* ***(C-F)*** *pro-inflammatory cytokine (IL-1β, CCL2, IL-6 and TNF-α) levels in RAW macrophages. All results are presented as Mean ± SEM (n=3) and analyzed by one-way ANOVA ***p<0.001; **p<0.01 vs control and ###p<0.001; ##p<0.01; #p<0.05 vs NETs.*

4. Discussion

AI/ML has brought a breakthrough in drug discovery through its improved predictive approaches for clinical translation of small molecules[52,53]. PAD4 enzyme converts arginine to citrulline, thereby, leading to NET release[40]. The NETs play a dual role in various diseases, it helps in the functioning of the innate immune system by killing microbes and facilitating exposure between its antimicrobial proteins and pathogens facilitating their clearance. However, their excessive formation causes tissue damage and organ dysfunction in both infectious and non-infectious condition[63,64]. We investigated a series of compounds from the Enamine Hit Locator Library against the PAD4 crystal structure (PDB ID: 8GOD) using

protein-based AI/ML virtual screening to identify a lead molecule as a highly potent PAD4 inhibitor. Most of the inhibitors developed against PAD4 proteins are targeted towards canonical site[57]. After detailed investigation of the PAD4 crystal structure, we found that there are adjacent pocket binding regions in its structure besides these canonical sites which are available for substrate binding and are not extensively explored. Potent PAD4 inhibitors present in ChEMBL database exhibited high binding towards these non-substrate competitive binding pockets, which were then selected as the target sites for virtual screening of 460,000 lead-like compounds from Enamine HLL. Molecular docking-based Auto Dock-GPU scores with machine learning (ML)-based scoring (Random Forest method) model trained on protein-ligand complexes were used for AI-assisted hit prioritization and compound selection[55]. Hydrogen bonds, hydrophobic interactions, and residue-level interactions were examined to identify conserved interaction patterns associated with stable ligand binding.

As a result, 25 hit molecules were selected for further pharmacological validation using the PAD4 inhibition kit and cell-based assays for estimating NET inhibition by SYTOX Green assay. PAD4 inhibition IC_{50} value of compounds 16 and 24 were found to be more potent than standard CLA, and these results were correlated with 5-fold increase in NETs inhibition by compounds 16 and 24 as compared to CLA respectively. Out of 25 hits, we selected compounds 16 and 24 for detailed NET and inflammation-related studies. In line with this, we found that compounds 16 and 24 exhibited similar binding energies, hydrogen and hydrophobic interactions with K3X (Co-crystal ligand) against the PAD4 crystal structure (PDB ID: 8GOD). Further, these selected compounds 16 and 24 were used for studying their anti-NET and anti-inflammatory effects in vitro evaluation in neutrophils and RAW264.7 macrophages. As our experimental studies have shown that the selected compounds 16 and 24 demonstrated no cytotoxicity up to 100 µM concentration, we used 10 µM concentration for compounds 16 and 24 to compare against standard CLA at 100 µM where it demonstrated anti-NETs effects based on prior studies conducted in our lab[61]. We observed that compounds 16 and 24 significantly inhibited extracellular NETs release, as observed in SYTOX Green, Giemsa and DCFDA stainings surpassing standard CLA in dHL-60 cells, which was verified by a significant reduction in the immunopositivity and mRNA expression of NET markers: NE, MPO, PAD4 and CitH3, which are used as indicators for NETosis. The critical step in NET formation is through citrullination of histones by PAD4, and the released NETs are coated with granular enzymes such as NE and MPO. The reports say that NE-knockout mice did not form NETs[65] and mice with deficient serine protease inhibitor; *serpinB1*, which degrades NE showed higher NET levels[66]. In addition to this, neutrophils isolated from MPO-deficient or knock-out mice

showed inability to form NETs[65,67], suggesting its critical role. Inhibition of PAD4 have shown protective effect in pulmonary fibrosis[68], deep vein thrombosis[69], SARS-CoV-2 infection[70], cancer[71], peritonitis[72], arthritis[73] through NET inhibition and thereby reported to reduced citrullinated histones. Furthermore, primary neutrophils were also evaluated for the anti-NETs effect by the selected compounds 16 and 24, which also demonstrated reduced NETs and their related markers.

The NET-macrophage axis has emerged as an attractive target, as exacerbated pro-inflammatory mediators are caused by macrophages stimulated by NETs-induced tissue injury in inflammatory and infectious conditions[74]. Therefore, to investigate how NETs modulation via PAD4 inhibition could affect inflammation, we used a PMA-stimulated NETs-induced model in macrophages[61] to study the activity of compounds 16 and 24 in inflammation. Notably, macrophages treated with NETs isolated from compound 16, 24 and standard CLA-treated neutrophils exhibited a decrease in both cellular and mitochondrial oxidative stress. Previous studies have reported that NET-based activation in macrophages occurs through TLR4 activation and cytokine production[62]. We examined TLR4 expression to check modulation of polarisation after treatment with NET-rich supernatant from neutrophils. The decreased fluorescence intensity of ROS stainings in compound 16 and 24-treated NETs suggests reduced oxidative stress in macrophages. Along with this, there was significant downregulation in the TLR4/MyD88 expression, M1 marker CD86, and pro-inflammatory cytokine levels in comparison with PMA-stimulated NETs. Collectively, novel PAD4 inhibitors-treated NETs not only decreased upstream neutrophil activation, as confirmed by expression of NETs markers, but also controlled downstream NET-driven inflammation in macrophages. This research work can also be explored in understanding PADs-mediated pathological states such as rheumatoid arthritis, sepsis, pulmonary fibrosis, acute pancreatitis, and cancer, where both NETs and inflammation drive disease progression. Furthermore, we plan to advance these novel inhibitors into complex preclinical in vivo models to evaluate their safety, pharmacokinetics, and survival efficacy in PAD4-mediated diseases. In future, we believe that this novel PAD4 inhibitor scaffold with significant potency can be further optimised to find a promising therapeutic lead to mitigate NET-driven tissue injury in acute and chronic inflammatory diseases.

5. Conclusion

In short, we utilised computational methods and biological assays to identify a potent candidate that can control inflammatory cross-talk between neutrophils and macrophages by PAD4

inhibition. Compounds 16 and 24 have shown encouraging results in both kit- and cell-based NETs and inflammatory assays. In vitro findings demonstrated that compounds 16 and 24 suppressed NET-related markers and mitigated NET-mediated macrophage inflammation. Further, its preclinical evaluation needs to be done in in vivo disease models like sepsis, atherosclerosis, arthritis and acute lung injury to evaluate its potent anti-inflammatory effects in complex biological systems.

6. Author Contribution

PD performed the experiments, analysed the data, and drafted and revised the manuscript. RS and PY coordinated, performed in silico studies, and reviewed the manuscript. CG designed the study, corrected, and reviewed the manuscript. All authors read and approved the manuscript. All data were generated in-house, and no paper mill was used. All authors agree to be accountable for all aspects of the work, ensuring integrity and accuracy.

7. Data Availability

Data will be made available on request.

8. Acknowledgement

The authors acknowledge the Department of Pharmaceuticals, Ministry of Chemicals and Fertilizers, Government of India, for supporting the research activities at NIPER-Hyderabad, and the Indian Council of Medical Research (ICMR), Government of India, for the financial support to Dr. Chandraiah Godugu under the Small Grant of project file no. DDR/IIRP/2024-7715; Dated: 31-01-2024 and Intermediate Grant of project file no. EMDR/IG/14/2025-01748; Dated: 25-11-2025.

9. References

1. Tjin, C. C., Wissner, R. F., Jamali, H., Schepartz, A. & Ellman, J. A. Synthesis and Biological Evaluation of an Indazole-Based Selective Protein Arginine Deiminase 4 (PAD4) Inhibitor. *ACS Med. Chem. Lett.* **9**, 1013 (2018).

2. Kearney, P. L. *et al.* Kinetic characterization of protein arginine deiminase 4: a transcriptional corepressor implicated in the onset and progression of rheumatoid arthritis. *ACS Publ. Kearney, M Bhatia, NG Jones, L Yuan, MC Glas. KL Catchings, M YamadaBiochemistry, 2005•ACS Publ.* **44**, 10570–10582 (2005).

3. Jones, J., Causey, C., opinion in …, B. K.-C. & undefined 2009. Protein arginine deiminase 4 (PAD4): Current understanding and future therapeutic potential. *pmc.ncbi.nlm.nih.govJ Jones,*

C Causey, B Knuckley, JL Slack-Noyes, PR ThompsonCurrent Opin. drug Discov. Dev. 2009•pmc.ncbi.nlm.nih.gov https://pmc.ncbi.nlm.nih.gov/articles/PMC3771078/.

4. Bicker, K. L. & Thompson, P. R. The protein arginine deiminases: Structure, function, inhibition, and disease. *Wiley Online Libr. Bicker, PR ThompsonBiopolymers, 2013•Wiley Online Libr.* **99**, 155–163 (2013).

5. Moscarello, M. A., Pritzker, L., Mastronardi, F. G. & Wood, D. D. Peptidylarginine deiminase: A candidate factor in demyelinating disease. *J. Neurochem.* **81**, 335–343 (2002).

6. Makrygiannakis, D. *et al.* Citrullination is an inflammation-dependent process. *Ann. Rheum. Dis.* **65**, 1219–1222 (2006).

7. Yue, J. *et al.* Inhibition of neutrophil extracellular traps alleviates blood-brain barrier disruption and cognitive dysfunction via Wnt3/β-catenin/TCF4 signaling in sepsis-associated encephalopathy. *J. Neuroinflammation* **22**, (2025).

8. Aslankoc, R., Savran, M., Ozmen, O. & Asci, S. Hippocampus and cerebellum damage in sepsis induced by lipopolysaccharide in aged rats - Pregabalin can prevent damage. *Biomed. Pharmacother.* **108**, 1384–1392 (2018).

9. Mei, B., Li, J. & Zuo, Z. Dexmedetomidine attenuates sepsis-associated inflammation and encephalopathy via central $α$2A adrenoceptor. *Brain. Behav. Immun.* **91**, 296–314 (2021).

10. Manda-Handzlik, A. & Demkow, U. The Brain Entangled: The Contribution of Neutrophil Extracellular Traps to the Diseases of the Central Nervous System. *Cells 2019, Vol. 8, Page 1477* **8**, 1477 (2019).

11. Tian, Y. *et al.* Peptidylarginine deiminase 2 has potential as both a biomarker and therapeutic target of sepsis. *JCI insight* **5**, (2020).

12. Zhao, T. *et al.* Protective effect of Cl-amidine against CLP-induced lethal septic shock in mice. *Sci. Rep.* **6**, 36696 (2016).

13. Witalison, E., Thompson, P. & Hofseth, L. Protein Arginine Deiminases and Associated Citrullination: Physiological Functions and Diseases Associated with Dysregulation. *Curr. Drug Targets* **16**, 700–710 (2015).

14. Zhou, J. *et al.* Peptidylarginine Deiminase 2 Knockout Improves Survival in hemorrhagic shock. *Shock* **54**, 458–463 (2020).

15. Fuhrmann, J., Clancy, K. W. & Thompson, P. R. Chemical Biology of Protein Arginine Modifications in Epigenetic Regulation. *Chem. Rev.* **115**, 5413 (2015).

16. Biron, B. M. *et al.* Cl-Amidine Prevents Histone 3 Citrullination and Neutrophil Extracellular Trap Formation, and Improves Survival in a Murine Sepsis Model. *J. Innate Immun.* **9**,.

17. Meng, W. *et al.* Depletion of neutrophil extracellular traps in vivo results in hypersusceptibility to polymicrobial sepsis in mice. *Crit. Care* **16**, R137 (2012).

18. Brinkmann, V. *et al.* Neutrophil extracellular traps kill bacteria. *Science* **303**, 1532–1535 (2004).

19. Zhai, R. *et al.* Neutrophil extracellular traps promote invasion and metastasis via NLRP3-mediated oral squamous cell carcinoma pyroptosis inhibition. *Cell Death Discov. 2024 101* **10**, 214- (2024).

20. Yousefi, S. & Simon, H. U. NETosis – Does It Really Represent Nature's "Suicide Bomber"? *Front. Immunol.* **7**, 328 (2016).

21. Ghosh, S. & Karin, M. Missing pieces in the NF-κB puzzle. *Cell* **109**, (2002).

22. Kawai, T. & Akira, S. The role of pattern-recognition receptors in innate immunity: update on Toll-like receptors. *Nat. Immunol.* **11**, 373–384 (2010).

23. Yamamoto, M. *et al.* Essential role for TIRAP in activation of the signalling cascade shared by TLR2 and TLR4. *Nature* **420**, 324–329 (2002).

24. Van Der Poll, T., Van De Veerdonk, F. L., Scicluna, B. P. & Netea, M. G. The immunopathology of sepsis and potential therapeutic targets. *Nat. Rev. Immunol.* **17**, 407–420 (2017).

25. He, W. *et al.* Forsythiaside B ameliorates coagulopathies in a rat model of sepsis through inhibition of the formation of PAD4-dependent neutrophil extracellular traps. *Front. Pharmacol.* **13**, 1022985 (2022).

26. McDonald, B. *et al.* Platelets and neutrophil extracellular traps collaborate to promote intravascular coagulation during sepsis in mice. *Blood* **129**, 1357–1367 (2017).

27. Arora, J., Mendelson, A. A. & Fox-Robichaud, A. Sepsis: network pathophysiology and implications for early diagnosis. *Am. J. Physiol. - Regul. Integr. Comp. Physiol.* **324**, R613 (2023).

28. Knight, J. S. *et al.* Peptidylarginine deiminase inhibition is immunomodulatory and vasculoprotective in murine lupus. *J. Clin. Invest.* **123**, 2981–2993 (2013).

29. Muth, A. *et al.* Development of a selective inhibitor of Protein Arginine Deiminase 2. *J. Med. Chem.* **60**, 3198 (2017).

30. Chumanevich, A. P. A. A. *et al.* Suppression of colitis in mice by Cl-amidine: A novel peptidylarginine deiminase inhibitor. *Am. J. Physiol. - Gastrointest. Liver Physiol.* **300**, 929–938 (2011).

31. Franck, G. *et al.* Roles of PAD4 and netosis in experimental atherosclerosis and arterial injury implications for superfcial erosion. *Circ. Res.* **123**, 33–42 (2018).

32. Soehnlein, O. Multiple roles for neutrophils in atherosclerosis. *Circ. Res.* **110**, 875–888 (2012).

33. Willis, V., Gizinski, A., … N. B.-T. J. of & 2011, undefined. N-α-Benzoyl-N5-(2-Chloro-1-Iminoethyl)-l-Ornithine Amide, a Protein Arginine Deiminase Inhibitor, Reduces the Severity of Murine Collagen-Induced Arthritis. *Acad. Willis, AM Gizinski, NK Banda, CP Causey, B Knuckley, KN Cordova, Y Luo, B LevittThe J. Immunol. 2011•academic.oup.com* https://academic.oup.com/jimmunol/article-abstract/186/7/4396/7990187.

34. Alturki, M. S. *et al.* A Multifaceted Computational Approach to Identify PAD4 Inhibitors for the Treatment of Rheumatoid Arthritis (RA). *Metabolites* **15**, 156 (2025).

35. Kawalkowska, J. *et al.* Abrogation of collagen-induced arthritis by a peptidyl arginine deiminase inhibitor is associated with modulation of T cell-mediated immune responses. *Sci. Reports 2016 61* **6**, 26430- (2016).

36. Moscarello, M. A. *et al.* Inhibition of peptidyl-arginine deiminases reverses protein-hypercitrullination and disease in mouse models of multiple sclerosis. *DMM Dis. Model. Mech.* **6**, 467–478 (2013).

37. Simon, D. I. & Zidar, D. Neutrophils in Atherosclerosis: Alarmin Evidence of a Hit and Run? *Circ. Res.* **110**, 1036 (2012).

38. Reis, L. R., Nascimento, R. O., Massafera, M. P., Di Mascio, P. & Ronsein, G. E. Investigating neutrophil responses to stimuli: Comparative analysis of reactive species-dependent and independent mechanisms. *Redox Biol.* **81**, 103540 (2025).

39. Liu, Y. *et al.* Peptidylarginine deiminases 2 and 4 modulate innate and adaptive immune responses in TLR-7–dependent lupus. *JCI Insight* **3**, (2018).

40. Knight, J. S. *et al.* Peptidylarginine deiminase inhibition disrupts NET formation and protects against kidney, skin and vascular disease in lupus-prone MRL/lpr mice. *Ann. Rheum. Dis.* **74**, 2199–2206 (2015).

41. Raup-Konsavage, W. M. *et al.* Neutrophil peptidyl arginine deiminase-4 has a pivotal role in ischemia/reperfusion-induced acute kidney injury. *Kidney Int.* **93**, 365–374 (2018).

42. Siddiqui, A. Z. *et al.* Cl-Amidine Improves Survival and Attenuates Kidney Injury in a Rabbit

Model of Endotoxic Shock. *Surg. Infect. (Larchmt).* **22**, 421–426 (2021).

43. Wang, B., Su, X., Zhang, B. & Pan, S. GSK484, an inhibitor of peptidyl arginine deiminase 4, increases the radiosensitivity of colorectal cancer and inhibits neutrophil extracellular traps. *J. Gene Med.* **25**, e3530 (2023).

44. Hu, Z. *et al.* Inhibition of NETosis via PAD4 alleviated inflammation in giant cell myocarditis. *iScience* **26**, 107162 (2023).

45. Ye, H. *et al.* Internalisation of neutrophils extracellular traps by macrophages aggravate rheumatoid arthritis via Rab5a. *RMD Open* **10**, e003847 (2024).

46. Xie, K. *et al.* The PAD4 inhibitor GSK484 diminishes neutrophil extracellular trap in the colon mucosa but fails to improve inflammatory biomarkers in experimental colitis. *Biosci. Rep.* **45**, 375 (2025).

47. Deng, H. *et al.* A Novel Selective Inhibitor JBI-589 Targets PAD4-Mediated Neutrophil Migration to Suppress Tumor Progression. *Cancer Res.* **82**, 3561–3572 (2022).

48. Heger, L. A. *et al.* Inhibition of protein arginine deiminase 4 prevents inflammation-mediated heart failure in arthritis. *Life Sci. Alliance* **6**, e202302055 (2023).

49. Gajendran, C. *et al.* Alleviation of arthritis through prevention of neutrophil extracellular traps by an orally available inhibitor of protein arginine deiminase 4. *Sci. Reports 2023 131* **13**, 3189-- (2023).

50. Patel, V. & Shah, M. Artificial intelligence and machine learning in drug discovery and development. *Intell. Med.* **2**, 134–140 (2022).

51. Kumar, B. S. *et al.* Machine learning guided virtual screening of FDA approved drugs targeting GSK-3$β$ in Alzheimer's disease. *Sci. Reports 2025 151* **15**, 45762-- (2025).

52. Ferreira, F. J. N. & Carneiro, A. S. AI-Driven DrugDiscovery: A Comprehensive Review. *ACS Omega* **10**, 23889–23903 (2025).

53. Verma, V. & Kumar, D. Artificial intelligence and machine learning in drug discovery: From lead discovery to clinical validation (2020–2025). *Lett. Drug Des. Discov.* **22**, 100341 (2025).

54. Paul, D. *et al.* Artificial intelligence in drug discovery and development. *Drug Discov. Today* **26**, 80 (2020).

55. Santos-Martins, D. *et al.* Accelerating AutoDock4 with GPUs and Gradient-Based Local Search. *J. Chem. Theory Comput.* **17**, 1060–1073 (2021).

56. Panda, B. *et al.* Peptidyl arginine deiminase-4 inhibitor ameliorates pulmonary fibrosis through

positive regulation of developmental endothelial locus-1. *Int. Immunopharmacol.* **140**, (2024).

57. Arita, K. *et al.* Structural basis for Ca(2+)-induced activation of human PAD4. *Nat. Struct. Mol. Biol.* **11**, 777–783 (2004).

58. Zdrazil, B. *et al.* The ChEMBL Database in 2023: a drug discovery platform spanning multiple bioactivity data types and time periods. *Nucleic Acids Res.* **52**, D1180–D1192 (2024).

59. Kuwahara, H. & Gao, X. Analysis of the effects of related fingerprints on molecular similarity using an eigenvalue entropy approach. *J. Cheminform.* **13**, (2021).

60. Kumar, B. S. *et al.* Machine learning guided virtual screening of FDA approved drugs targeting GSK-3β in Alzheimer's disease. *Sci. Reports 2025 151* **15**, 45762- (2025).

61. Panda, B., Chilvery, S., Devi, P., Kalmegh, R. & Godugu, C. Inhibition of peptidyl arginine deiminase-4 ameliorated pulmonary fibrosis via modulating M1/M2 polarisation of macrophages. *Life Sci.* **362**, 123354 (2025).

62. Simonson Gonçalves, B. *et al.* Neutrophil extracellular traps promote macrophage activation through Toll-like receptor engagement and PKA and NF-kB signaling pathways. *Cell Commun. Signal. 2026 241* **24**, 419-- (2026).

63. Zhu, S. *et al.* Neutrophil extracellular traps contribute to immunothrombosis formation via the STING pathway in sepsis-associated lung injury. *Cell Death Discov. 2023 91* **9**, 315- (2023).

64. Tu, H. *et al.* Dying to Defend: Neutrophil Death Pathways and their Implications in Immunity. *Adv. Sci.* **11**, 2306457 (2024).

65. Papayannopoulos, V., Metzler, K. D., Hakkim, A. & Zychlinsky, A. Neutrophil elastase and myeloperoxidase regulate the formation of neutrophil extracellular traps. *J. Cell Biol.* **191**, 677–691 (2010).

66. Farley, K., Stolley, J. M., Zhao, P., Cooley, J. & Remold-O'Donnell, E. A SerpinB1 Regulatory Mechanism Is Essential for Restricting Neutrophil Extracellular Trap Generation. *J. Immunol.* **189**, 4574–4581 (2012).

67. Metzler, K. D. *et al.* Myeloperoxidase is required for neutrophil extracellular trap formation: implications for innate immunity. *Blood* **117**, 953–959 (2011).

68. Panda, B. *et al.* Peptidyl arginine deiminase-4 inhibitor ameliorates pulmonary fibrosis through positive regulation of developmental endothelial locus-1. *Int. Immunopharmacol.* **140**, 112861 (2024).

69. Martinod, K. *et al.* Neutrophil histone modification by peptidylarginine deiminase 4 is critical

for deep vein thrombosis in mice. *Proc. Natl. Acad. Sci. U. S. A.* **110**, 8674–8679 (2013).

70. Bonilha, C. S. *et al.* PAD4 inhibition impacts immune responses in SARS-CoV-2 infection. *Mucosal Immunol.* **18**, 861–873 (2025).

71. Pitter, M. R. *et al.* PAD4 controls tumor immunity via restraining the MHC class II machinery in macrophages. *Cell Rep.* **43**, 113942 (2024).

72. Cani, E. *et al.* Impact of peptidylarginine deiminase 4 (PAD4) deficiency in a fecal-induced peritonitis model of sepsis. *J. Thromb. Haemost.* **23**, 2342–2355 (2025).

73. Gajendran, C. *et al.* Alleviation of arthritis through prevention of neutrophil extracellular traps by an orally available inhibitor of protein arginine deiminase 4. *Sci. Rep.* **13**, (2023).

74. Shan, X. *et al.* Interactions between neutrophil extracellular traps and macrophages: the key to inflammatory diseases. *Front. Immunol.* **17**, 1731687 (2026).